Journal of Molecular Liquids 431 (2025) 127676

Contents lists available at ScienceDirect

Journal of Molecular Liquids

journal homepage: www.elsevier.com/locate/molliq

Different impact of menthol chirality on ideal and deep eutectic solvents: Thermal and structural insights

Giorgia Mannucci [a], Matteo Busato [a,*], Eva Pietropaoli [a], Matteo Palluzzi [a], Paolo Casu [a], Angela Capocefalo [b], Claudia Fasolato [c], Paolo Postorino [d], Paola D'Angelo [a,*]

[a] Department of Chemistry, Sapienza University of Rome, P.le A. Moro 5, Rome, 00185, Italy
[b] Department of Physical and Chemical Sciences, University of L'Aquila, Via Vetoio Coppito, L'Aquila, 67100, Italy
[c] Institute for Complex Systems, National Research Council, c/o Department of Physics, Sapienza University of Rome, P.le A. Moro 5, Rome, 00185, Italy
[d] Department of Physics, Sapienza University of Rome, P.le A. Moro 5, Rome, 00185, Italy

ARTICLE INFO

Keywords:
Hydrophobic deep eutectic solvents
Chirality
Enantiomers
Menthol
Butylated hydroxytoluene
Thymol
Molecular dynamics
X-ray scattering

ABSTRACT

Although chiral molecules are common components of deep eutectic solvents (DESs), the impact of precursor chirality on the fundamental aspects of these solvents is far from being systematically explored. Here, the effect of chirality on the eutectic mixtures formed by the optically active menthol (MEN) with thymol (TYM) and butylated hydroxytoluene (BHT) has been investigated. To this purpose, we resorted to a combined thermal and structural analysis by means of differential scanning calorimetry measurements aided by the COSMO-RS solvation model, Raman spectroscopy, small- and wide-angle X-ray scattering, and molecular dynamics simulations. A slightly different thermal behavior and self-association are observed for the levorotatory enantiomer (L-MEN) as compared to the dextrorotatory one (D-MEN) and the racemate (D/L-MEN) in the pure MEN system. This behavior is preserved in the BHT:MEN 1:3 ideal eutectic as the interaction with the BHT molecules is hampered due to the presence of the bulky substituents. On the other hand, the precursor chirality has no detectable influence on the overall properties of the TYM:MEN 1:1 DES due to strong interactions with the non-chiral counterpart. These findings have important implications for the design and employment of chiral DESs for enantioselective purposes.

1. Introduction

Deep eutectic solvents (DESs) have recently emerged as multipurpose innovative media due to an environmentally friendly pedigree and unique chemical-physical properties [1,2]. Although the definition of these systems is still controversial, they are currently conceived as mixtures showing a melting point (MP) depression as compared to the predicted one assuming thermodynamic ideality for the solid-liquid equilibrium (SLE) between the precursors [3]. This thermal behavior is deemed reliant on the stronger intermolecular interactions between the mixed components as compared to those established in their pure states. Such interplay is often due to the H-bonding, although interactions of other nature, such as halogen bonding or dispersion forces, and entropic factors, have been found to contribute to or even dominate the MP depression [4–7].

DES physicochemical properties can be tuned through judicious choice of the precursors and/or their molar ratio, meeting the concept of "designing" solvents [2]. These components are typically classified into five types (I-V) based on their chemical nature, with type V constituted by non-ionic molecular compounds only [1,2]. Apart from sharing the main properties of types I-IV, DESs belonging to this more recent class often display lower viscosities, are chloride-free, and hydrophobic [8]. As a result, they are particularly suitable for liquid-liquid extractions of target compounds like pesticides [9], biomolecules [10,11], and metal species [12–17] from aqueous solutions, in alternative to traditional organic solvents.

Terpenes are a class of natural products and versatile constituents of type V DESs [18,19]. Among them, menthol (MEN) is the most frequently employed as it forms eutectic mixtures with many other precursors that find use across various fields [10,8]. MEN-based DESs are

* Corresponding authors.
E-mail addresses: matteo.busato@uniroma1.it (M. Busato), p.dangelo@uniroma1.it (P. D'Angelo).

https://doi.org/10.1016/j.molliq.2025.127676
Received 23 October 2024; Received in revised form 7 April 2025; Accepted 24 April 2025
Available online 29 April 2025

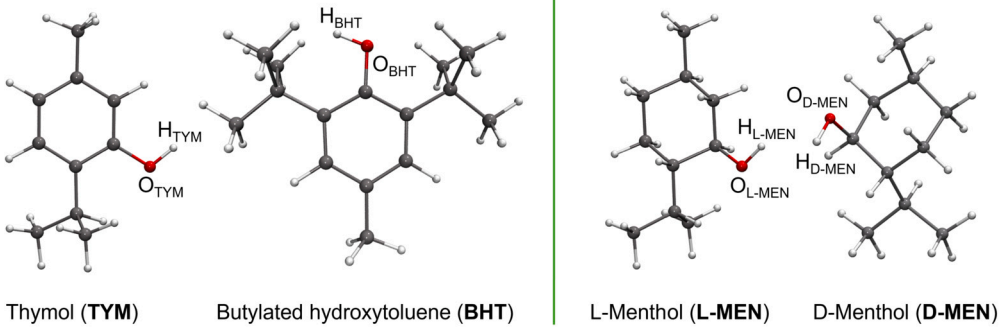

Fig. 1. Molecular structures of thymol (TYM), butylated hydroxytoluene (BHT), L-menthol (L-MEN), and D-menthol (D-MEN) (white, hydrogen; gray, carbon; red, oxygen).

also promising biocompatible options for pharmaceutical applications, in particular as carriers for drug delivery systems [20–24]. MEN exists in two optical isomers: the levorotatory (1*R*,2*S*,5*R*)(-)-MEN (L-MEN), derived from natural sources, and the dextrorotatory (1*S*,2*R*,5*S*)-(+)-MEN (D-MEN), primarily synthesized chemically [25]. Other common DES components are naturally occurring chiral molecules, such as amino acids, sugars, and carboxylic acids [8,26,27]. Chiral DESs have been therefore proposed for enantioselective extraction processes [28], electroanalysis [29,30], as organocatalytic reaction media [31,32], and chiral solvents for circularly polarized luminescence [33,34]. Aside from practical aspects, the structural properties of MEN racemic mixtures with acetic, lauric, and pyruvic acid have been investigated, and the number of H-bonds formed by L-MEN with the counterpart molecules was found higher than those established by D-MEN [28]. This is a surprising result, as enantiomers can be separated through stereoselectivity owing to their different interaction with another chiral molecule, while the other physicochemical properties should be identical. On the other hand, the overall structure was shown to remain the same for choline chloride mixtures with either single enantiomeric or racemic tartaric acid, with small differences in interactions only between the different enantiomers [27]. Understanding whether the chirality of the parent compounds can influence the structural properties or alter the primary interactions in the solvent appears, therefore, crucial. However, to the best of our knowledge, papers addressing the impact of precursor chirality at a molecular level remain scarce, while new knowledge could significantly benefit from a more systematic investigation of these fundamental aspects.

Here, we present a comprehensive study on the structural and thermal properties of MEN-based eutectic mixtures as a function of MEN chirality. First, the L-MEN and D-MEN enantiomers were characterized and compared to the racemic compound, corresponding to an equimolar mixture of D- and L-MEN (D/L-MEN). Subsequently, MEN mixtures with thymol (TYM) and butylated hydroxytoluene (BHT) were characterized. The molecular structures of these components are reported in Fig. 1. The TYM:L-MEN system represents the archetypal type V DES and shows a massive MP depression, maximized around the 1:1 molar ratio [35]. On the other hand, the BHT:L-MEN system was previously classified as an ideal eutectic with a MP close to room temperature for the 1:3 composition [9,5,6]. The first behavior is due to the dominating TYM-L-MEN H-bond, where the TYM molecule behaves as an H-bond donor (HBD) towards the L-MEN one, acting as H-bond acceptor (HBA), both through their hydroxyl groups. Conversely, the sterically hindered hydroxyl moiety of the BHT molecule is responsible for its negligible H-bonds in the BHT:L-MEN mixture, where interactions among L-MEN molecules predominate and a thermal behavior close to ideality is obtained as a result. Therefore, it is of great interest to assess the impact of MEN chirality on these two antipodal systems. To this purpose, TYM:MEN 1:1 and BHT:MEN 1:3 mixtures, where MEN corresponds either to L-MEN, D/L-MEN, or D-MEN, were studied combining experimental techniques like differential scanning calorimetry (DSC), Raman spectroscopy, small- and wide-angle X-ray scattering (SWAXS), with molecular dynamics (MD) simulations and the COSMO-RS solvation model. Accurate information about the properties of the inspected systems is obtained through this multidisciplinary approach, opening a better perspective for potential enantioselective processes employing optically active DESs.

2. Materials and methods

2.1. Chemicals and sample preparation

L-MEN (natural source, food grade, ≥ 99%), D-MEN (≥ 99%), D/L-MEN (≥ 98%), BHT (food grade, ≥ 99%), and TYM (≥ 98.5%) were purchased from Merck Life Science S.r.l. TYM:MEN and BHT:MEN mixtures at 1:1 and 1:3 molar ratios, respectively, where MEN = L-MEN, D/L-MEN, and D-MEN, were prepared by mixing the desired amount of the starting compounds in glass vials and then heating at about 333 K until homogeneous transparent liquids were obtained. Given the hygroscopicity of the D/L-MEN and D-MEN compounds, these mixtures were prepared in an Ar-filled glove box with water content below 10 ppm. The experimental densities at room temperature of the mixtures were measured by weighing a sample amount of 1 mL in a volumetric flask on an analytical balance. Three measurements were performed and averaged. The resulting densities are listed in Table S1 of the Supporting Information (SI).

2.2. DSC experiments

DSC thermograms were collected for the L-MEN, D/L-MEN, and D-MEN compounds, and for the BHT:L-MEN, BHT:D/L-MEN, and BHT:D-MEN mixtures at a 1:3 molar ratio using a DSC821 instrument (Mettler-Toledo, Columbus, USA). A sample amount of about 10 mg was weighed and then sealed in a 40 μL aluminum pan. Samples were cooled from room temperature to 248 K at a rate of -5 K min^{-1}, followed by a heating ramp to 333 at 2 K min^{-1}. During all measurements, the furnace was purged with dry nitrogen at a flow rate of 60 mL min^{-1}. The MP temperature (T_m) of each mixture was taken as the maximum value of the melting peak. The error in the MP measurement amounts to 1.8% and was determined through three repetitions of the measurement on the same sample.

2.3. Raman spectroscopy measurements

Raman spectra were collected at the HPS laboratory of the Sapienza University of Rome using a Horiba HR-Evolution microspectrometer in backscattering geometry. The system was equipped with a solid-state laser (λ = 532 nm, 90 mW power at the sample surface) and a set of neutral attenuating optical filters to prevent laser heating and sample

degradation. The detector was a Peltier-cooled charge-coupled device (CCD), providing a spectral resolution better than 3 cm^{-1}, thanks to a 600 groove/mm grating with an 800 mm focal length. The elastically scattered light was removed using an optical filtering system comprised of three volume Brag grating notch filters [36]. The spectrometer was coupled with a confocal microscope equipped with a variety of interchangeable objectives. The spectra were collected in the O-H stretching (ν_{OH}) region (3100 - 3700 cm^{-1}) in quartz capillaries with 1.5 mm diameter at 333 K using a Peltier thermostated cell. A cubic baseline subtraction was applied to all the spectra, which were then normalized as described in the text.

2.4. SWAXS measurements

SWAXS spectra were collected at the CoSAXS beamline [37] of the MAX IV Laboratory synchrotron facility (Lund, Sweden) using an Eiger2 4M detector for the SAXS region and a Pilatus L-shaped 2M Mythen 12 for the WAXS one. Data were acquired at room temperature for the TYM:L-MEN, TYM:D/L-MEN, and TYM:D-MEN mixtures at a 1:1 molar ratio, and for the BHT:L-MEN, BHT:D/L-MEN, and BHT:D-MEN mixtures at a 1:3 molar ratio. A silver behenate standard was used to calibrate the scattering vector q-range. An overall explored q-region of 0.03 - 3.00 $Å^{-1}$ was obtained as a result of different sample-detector distances and an X-ray beam with an energy of 18.0 keV. The recorded 2D detector images were subtracted for the dark counts and then masked, azimuthally averaged, normalized for the transmitted beam intensity, exposure time, and subtended solid angle per pixel, and then averaged. The empty capillary contributions were subtracted and the different angular ranges were merged with the SAXSutilities2 [38] and Primus [39] packages.

2.5. Computational details

Classical MD simulations were carried out on the L-MEN, D/L-MEN, and D-MEN compounds, on the TYM:MEN mixtures at a 1:1 molar ratio, and on the BHT:MEN mixtures at a 1:3 molar ratio, with MEN = L-MEN, D/L-MEN, and D-MEN. Periodic cubic boxes with approximately 50 Å side lengths were built with initial atomic positions randomized by the PACKMOL package [40] and the number of species selected to reproduce the density of each system. The experimental density measured at 298 K was employed for the mixtures, while the densities of D-MEN and D/L-MEN were assumed to be equivalent to that of L-MEN at 333 K [41]. Further details regarding the simulated systems can be found in Table S1. After energy minimization, the system equilibration was conducted in the NVT ensemble with a heating ramp from 298 to 500 K over 10 ns, and then cooling down for a total time of 20 ns. Production runs for data analysis were performed for 50 ns under NVT at 333 K for the MEN compounds and 298 K for the mixtures, as these temperatures are above the experimental MPs (*vide infra*). Temperature control was obtained using the Nosé-Hoover thermostat with a relaxation constant of 0.5 ps. Integration of the equation of motion was performed by the leap-frog algorithm, utilizing a time step of 1.0 fs. The LINCS algorithm [42] was applied to constrain all stretching vibrations involving hydrogen atoms. All simulations and analyses were conducted using the Gromacs 2020.6 program [43]. The VMD 1.9.3 software was used for trajectory visualization [44].

Structures and interactions of the BHT and TYM molecules were represented by the all-atom optimized potentials for liquid simulations (OPLS-AA) force field [45]. For the L-MEN and D-MEN molecules the OPLS-compatible parameters developed by Jasik et al. [46] were employed. The long-range electrostatic forces were computed using the particle mesh Ewald method, employing a cutoff radius of 12 Å for all non-bonded interactions [47,48]. Cross-terms for the Lennard-Jones interactions were built with the Lorentz-Berthelot combining rules. The partial charges for the L-MEN, D-MEN, BHT, and TYM molecules were calculated with the CHELPG scheme [49]. To this purpose, geometry optimizations of the isolated molecules in gas phase conditions were carried out at the density functional theory (DFT) level using the B3LYP functional [50] in combination with the 6-31G(d,p) basis set. The Gaussian 16 package [51] was used for DFT simulations.

Table 1
MP temperature T_m determined by DSC measurements for the L-MEN, D/L-MEN, and D-MEN compounds, BHT:MEN 1:3 mixtures, and calculated by the COSMO-RS method for the TYM:MEN 1:1 mixtures, with MEN = L-MEN, D/L-MEN, and D-MEN. The statistical errors are equal to the 1.8% for the DSC measurements and to 7 K for the COSMO-RS related calculations [63].

System	T_m (K)
L-MEN	317.0
D/L-MEN	307.9
D-MEN	315.3
TYM:L-MEN	264.4
TYM:D/L-MEN	267.4
TYM:D-MEN	268.9
BHT:L-MEN	297.4
BHT:D/L-MEN	293.6
BHT:D-MEN	297.7

The thermal properties of the TYM:MEN 1:1 mixtures with MEN = L-MEN, D/L-MEN, and D-MEN, were obtained through the COSMO-RS solvation model. L-MEN, D-MEN, and TYM molecules were optimized by DFT calculations with the TURBOMOLE V4.5.2 package [52] using the COSMO solvation model with infinite permittivity, the B-P86 functional [53,54], and the def2_TZVPD [55,56] basis set. The COSMOtherm21 [57] software was used to perform all COSMO-RS-related calculations. The experimental thermal parameters for the pure precursors employed for the calculations are reported in Table S2.

3. Results and discussion

3.1. Comparative analysis of MEN enantiomers

A thorough characterization of the optically active components was first carried out to comprehend the impact of selecting a particular enantiomer as a precursor of an eutectic mixture. The DSC thermograms recorded for the heating stage of the L-MEN, D/L-MEN, and D-MEN compounds are shown in Fig. 2a. A well-defined endothermic peak is obtained in all cases, indicating a solid-liquid transition. The T_m values, taken at the minimum position of each peak, are listed in Table 1. L-MEN melts at 317.0 K, while D-MEN shows only a slightly lower MP of 315.3 K. On the other hand, the maximum of the melting peak for D/L-MEN stands at 307.9 K. This is consistent with the findings of Corvis et al. [25], who attributed the lower MP of D/L-MEN to a eutectic behavior driven by the mixing of the two enantiomers. Indeed, the phase diagram of D/L-MEN, derived by Corvis et al., classified this species as a racemic compound. Such mixtures always exhibit a negative contribution from the entropy of mixing [58], which consequently acts as the driving force for the melting point depression.

To get a deeper insight a structural analysis of the melt phase of the MEN precursors was carried out to assess if this thermal behavior could depend on interactions of different nature. To this purpose, the sensitivity of the Raman spectroscopy towards the O-H vibration has been exploited to retrieve information about the H-bonding association. Fig. 2b shows the ν_{OH} region of the spectra collected for the L-MEN, D/L-MEN, and D-MEN compounds in the liquid state. A first notable feature is a narrow high frequency peak in the 3600 - 3650 cm^{-1} spectral region. This contribution was previously associated with “free” hydroxyl groups not involved in H-bonding and labeled as α-OHs [59–62]. Hydroxyls behaving as HBAs through the oxygen atom, while not participating as

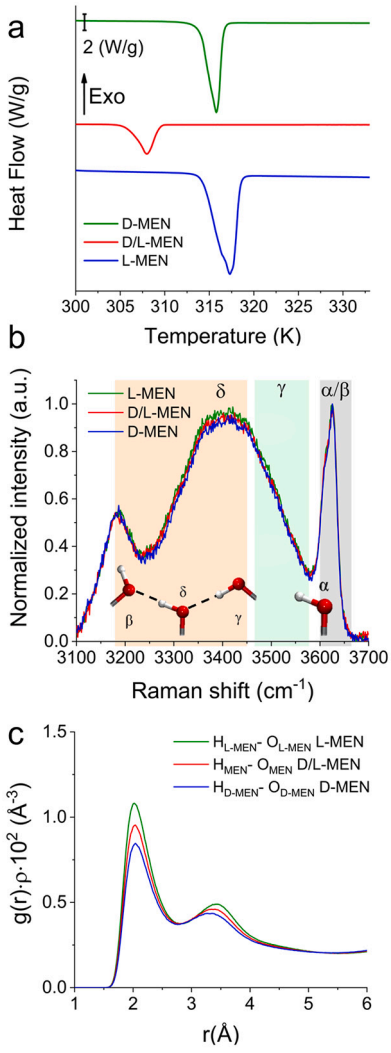

Fig. 2. a) Heating stage of DSC traces, b) ν_{OH} region of the Raman spectra at 333 K normalized for the maximum scattered intensity, and c) intermolecular H_{MEN}-O_{MEN} radial distribution functions multiplied by the numerical density of the observed atoms, $g(r)\rho$'s, calculated from the MD simulations at 333 K, for L-MEN (green), D/L-MEN (red), and D-MEN (blue). In the case of the D/L-MEN system, reference is referred to both L-MEN and D-MEN molecules. In Fig. 2b, the spectral ranges corresponding to the α/β-, γ-, and δ-OH contributions according to literature data [59–62] are highlighted on the background for the sake of clarity.

HBDs with the hydrogen one, are labeled as β-OHs and vibrate at similar frequencies. Besides this population of non- and weakly-interacting MEN molecules, the spectral profiles of all three systems are dominated by a broad band centered at approximately 3400 cm^{-1}. This lower frequency contribution can be associated with hydroxyl groups behaving contemporary as HBDs and HBAs, labeled as δ-OHs, and thus involved in H-bond networking [59,61,62,64–66]. This spectral evidence, therefore, indicates a high extent of self-association among MEN molecules in the precursor compounds. The broadness of this band also envelops the spectral region around ~3550 cm^{-1}, which is typically connected with terminal proton-donating hydroxyls with the lone pairs of the oxygen atom not involved in H-bonding, thus responsible for H-bonded dimers, and labeled as γ-OHs [59–61]. Note that a small decrease in the intensity of the whole ~3400 cm^{-1} contribution following the L-MEN > D/L-MEN > D-MEN sequence can be observed. Although these trends are small and barely emerge from the signal noise, a weakening of the H-bonding association is suggested when passing from the L-MEN to the D-MEN compounds, with the D/L-MEN sandwiched between them.

Table 2
Position of the first peak maximum r_{max} and integration number N calculated up to the reported cutoff distance for the intermolecular H_{MEN}-O_{MEN} and H_{TYM}-O_{MEN} $g(r)$'s obtained from the MD simulations of the MEN compounds at 333 K, of the TYM:MEN 1:1 and BHT:MEN 1:3 mixtures at 298 K, with MEN = L-MEN, D/L-MEN, and D-MEN. The errors on the distances and coordination numbers are 0.01 Å and 0.05, respectively.

System	$g(r)$	r_{max} (Å)	N	Cutoff (Å)
L-MEN	$H_{L\text{-}MEN}$-$O_{L\text{-}MEN}$	2.02	0.44	2.80
D/L-MEN	$H_{D/L\text{-}MEN}$-$O_{D/L\text{-}MEN}$	2.04	0.40	2.79
D-MEN	$H_{D\text{-}MEN}$-$O_{D\text{-}MEN}$	2.04	0.36	2.76
TYM:L-MEN	H_{TYM}-$O_{L\text{-}MEN}$	1.96	0.40	2.80
TYM:D/L-MEN	H_{TYM}-$O_{D/L\text{-}MEN}$	1.96	0.39	2.76
TYM:D-MEN	H_{TYM}-$O_{D\text{-}MEN}$	1.96	0.39	2.78
BHT:L-MEN	$H_{L\text{-}MEN}$-$O_{L\text{-}MEN}$	2.00	0.47	2.78
BHT:D/L-MEN	$H_{D/L\text{-}MEN}$-$O_{D/L\text{-}MEN}$	2.00	0.45	2.78
BHT:D-MEN	$H_{D\text{-}MEN}$-$O_{D\text{-}MEN}$	2.00	0.40	2.72

An atomistic description obtained from MD simulations helped us to deepen this aspect. Radial distribution functions ($g(r)$'s) for the intermolecular H_{MEN}-O_{MEN} atom pairs were calculated from the obtained trajectories, as this distribution is known to be a useful mark of H-bonding [35,5,6,67,68]. The obtained curves are reported in Fig. 2c and show similar shapes, *i.e.*, a well-defined first peak with a maximum at about 2.0 Å (Table 2), plus a broader peak of lower intensity around ~3.5 Å. This distribution is in line with those typically observed for strong and intrachain H-bonds [69,35,5,6]. It is noteworthy that the $g(r)$ intensity decreases following the L-MEN > D/L-MEN > D-MEN trend, as previously observed for the δ-OHs band from the Raman spectra (Fig. 2b). Since the mere visual comparison can be misleading when comparing $g(r)$'s, integration numbers N were calculated by integrating each curve up to a cutoff distance chosen at the first minimum and listed in Table 2. A value of 0.44 is obtained for L-MEN, indicating a high extent of self-aggregation among these molecules. This number is reduced to 0.36 for the D-MEN, while 0.40 is obtained for the racemic compound. The whole result suggests stronger H-bonds among L-MEN molecules compared to D-MEN, with the D/L-MEN compound standing in between because of L-MEN/D-MEN mixing. However, such small differences can hardly explain the obtained thermal behavior (Fig. 2a and Table 1). Differently, the lower MP of D/L-MEN is more likely dominated by entropic effects due to the mixing of the two enantiomers and agrees with an ideal eutectic behavior of the racemic compound [58]. Additional insights can be obtained from the $g(r)$ between the centers of mass (COM) of the molecules under investigation. As shown in Fig. S4, in the D-MEN system, the $g(r)$ between the COMs is the most intense, followed by that of D/L-MEN and L-MEN. This trend is opposite to that observed for the function associated with H-bonding, confirming previous observations. In fact, in L-MEN, due to a slightly higher degree of H-bond networking, the structural order is reduced.

3.2. Impact of MEN chirality on the eutectic mixtures: thermal behavior

TYM:MEN 1:1 and BHT:MEN 1:3 mixtures, with MEN being either L-MEN, D/L-MEN, or D-MEN, were characterized to investigate the influence of MEN chirality and assess whether the behavior of the parent enantiomers in their pure state is preserved even upon mixing with the counterparts. To this purpose, a thermal characterization of the solid-liquid equilibrium (SLE) between the precursors was first carried out. As far as the TYM:MEN 1:1 system is concerned, the experimental MP determination was not possible due to the absence of crystallization during the cooling stage of the DSC measurements, which prevented the achievement of a melting peak. This is a well-known drawback of many DESs that often present the formation of metastable phases, polymorphism, and the presence of solid solutions [70,71]. Under these circumstances, we exploited the predictive capability of the COSMO-RS solvation model, as this computational tool is typically aimed at

providing reliable thermal data circumventing such experimental drawbacks [63,72]. The phase diagram calculated for the TYM:L-MEN system was first compared with the literature data available for compositions far from the eutectic one [70] to assess the reliability of the simulation protocol. The results are shown in Fig. S1a and compared with the phase diagram traced assuming thermodynamic ideality. The simulation agrees well with the experimental outcome. A marked MP depression in comparison with the ideal phase diagram is observed for compositions approaching the eutectic one, in agreement with the classification of this mixture as a type V DES [70,35]. Once verified the goodness of the simulation, this method was employed to predict the phase diagrams also for the TYM:D/L-MEN and TYM:D-MEN systems. The results are shown in Fig. S1b and c, respectively. The SLE predicted by the COSMO-RS calculation is very similar in the three cases, irrespectively of the MEN enantiomer. A comparable picture is delivered by the T_m values calculated for the 1:1 composition (Table 1). The predicted MPs are 264.4 K for TYM:L-MEN, 267.4 K for TYM:D/L-MEN, and 268.9 K for TYM:D-MEN, thus falling within the error margin of this method (~7 K) [63].

The MPs for the BHT:MEN 1:3 mixtures were determined by DSC measurements, as melting peaks in the heating stage could be obtained owing to a successful crystallization during the cooling process (Fig. S2). The T_m values resulted 297.6, 293.6, and 297.7 K for BHT:L-MEN, BHT:D/L-MEN, and BHT:D-MEN, respectively (Table 1). The interesting outcome is that, although almost identical MPs are obtained for the BHT:L-MEN and BHT:D-MEN systems, the BHT:D/L-MEN one melts at a significantly lower temperature, within an experimental error of 1.8%. This behavior reminds what was found for the MEN precursors (Fig. 2a and Table 1), and is at variance with the TYM:MEN DES. Finally, to facilitate a comparison between the two systems, the SLE for the BHT:MEN system was also calculated (Fig. S6) using the COSMO-RS solvation model, yielding results that are in good agreement with the experimental data.

3.3. Impact of MEN chirality on the eutectic mixtures: H-bonding

A different thermal behavior was evidenced between the TYM:MEN and BHT:MEN mixtures as a function of the employed MEN precursor. A study of the H-bond interaction in these systems was carried out to assess if this is the case also from a structural point of view. Fig. 3a shows the ν_{OH} region of the Raman spectra collected for the TYM:MEN 1:1 mixtures with MEN = L-MEN, D/L-MEN, and D-MEN. The spectral profiles resulting from the mixing of these precursors are markedly different from pristine MEN (Fig. 2b), as the most intense band lies in the spectral region connected with γ-OHs. [59–61] Being these hydroxyls a mark of H-bonded dimers, this contribution can be connected with TYM molecules behaving as HBDs towards the MEN molecules, acting as HBAs. This interaction originates from the phenolic nature of TYM, which makes its hydroxyl group more positive due to resonance effects and the hydrogen atom a better donor, while the oxygen atom is a worse acceptor. [73,35] In contrast, the MEN molecule exhibits no resonance effects. Consequently, when these two compounds are mixed, the TYM-MEN donor-receptor interaction is established as the most favored one. In addition, bands in the δ-OHs and α/β-OHs regions can be distinguished. The key point is that the whole spectral profiles are almost superimposable for the three mixtures and indicate a similar H-bonding aggregation, independently of the employed MEN enantiomer.

A different situation is evidenced by the Raman spectra of the BHT:MEN 1:3 mixtures (Fig. 3b). These profiles differ from the TYM:MEN ones, as more pronounced bands in the high frequency region connected with α/β-OHs are obtained. This spectral evolution was previously associated with BHT addition to MEN resulting in an increase in the non-interacting hydroxyl population due to the sterically hindered BHT molecule. [5,6] On the other hand, the ~3400 cm^{-1} band connected with δ-OHs can be attributed to the persistent H-bond networking among MEN molecules. It is worth noting that this band shows a higher intensity for the BHT:L-MEN mixture than the BHT:D/L-MEN and

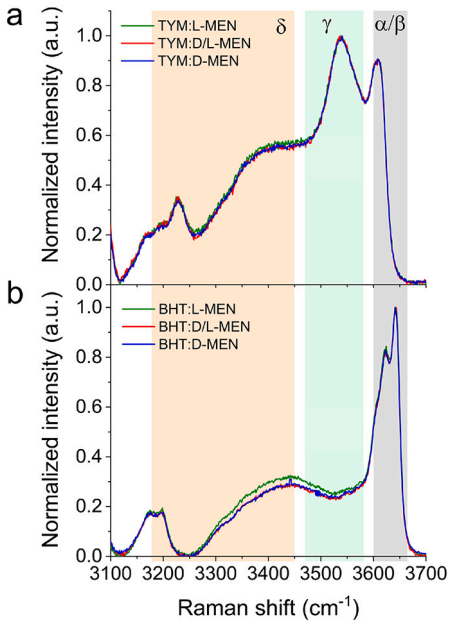

Fig. 3. ν_{OH} region of the Raman spectra at 333 K normalized for the maximum scattered intensity for the a) TYM:MEN 1:1 and b) BHT:MEN 1:3 mixtures with MEN = L-MEN (green), D/L-MEN (red), and D-MEN (blue). The spectral ranges corresponding to the α/β-, γ-, and δ-OH contributions according to literature data [59–62] are highlighted on the background for the sake of clarity.

BHT:D-MEN ones. This difference suggests greater H-bonding among L-MEN molecules compared to D-MEN even upon mixing with BHT and recalls the behavior shown by these precursors in their pristine form (Fig. 2b).

MD simulations of the TYM:MEN 1:1 and BHT:MEN 1:3 systems were carried out to obtain a possible confirmation of these trends. Fig. 4a illustrates the $g(r)$'s representative of the TYM-MEN donor-receptor H-bond in TYM:MEN 1:1 through the H_{TYM}-O_{MEN} atom pairs distribution. The obtained $g(r)$'s are almost superimposable, as is also testified by the calculated N values of 0.40 for TYM:L-MEN and 0.39 for both TYM:D/L-MEN and TYM:D-MEN (Table 2). This confirms that the TYM-MEN H-bond shows no selectivity for the chosen enantiomer, which is expected, as a non-chiral molecule like TYM should not be sensitive toward chirality. On the other hand, a clear decrease in the intensity of the H_{MEN}-O_{MEN} $g(r)$'s in the BHT:MEN 1:3 systems is observed following the L-MEN > D/L-MEN > D-MEN trend and the same is true when considering the integration numbers of 0.47, 0.45, and 0.40, respectively (Table 2). A similar result was obtained for the same distribution in the MEN precursors (Fig. 2c). The interpretation relies on the negligible H-bond interactions between the parent compounds previously observed for BHT:L-MEN mixtures, where the only established H-bonds are those between MEN molecules. [5,6] In this way, the different affinity among MEN enantiomers is preserved even upon mixing with BHT.

To confirm this observation, the H_{MEN}-O_{MEN} $g(r)$'s in the TYM:MEN 1:1 systems were also calculated to inspect the H-bond among the remaining MEN molecules, *i.e.*, those not interacting with TYM. The obtained functions decrease in intensity (Fig. S3), as also testified by the calculated N values (Table S3), following the TYM:L-MEN (0.31) > TYM:D/L-MEN (0.28) > TYM:D-MEN (0.26) trend. The higher affinity among L-MEN molecules previously observed in the pristine precursors is therefore retained also in the TYM:MEN 1:1 mixtures when dealing with the MEN-MEN interaction. However, this has no detectable influence on H-bonding as shown by Raman spectroscopy (Fig. 3a), and on the mixture thermal behavior (Fig. S1 and Table 1) due to the overwhelming TYM-MEN interaction.

These results are also confirmed by the calculation of the $g(r)$ between the COMs. In fact, in the BHT:MEN 1:3 system (Fig. S5a–c), the

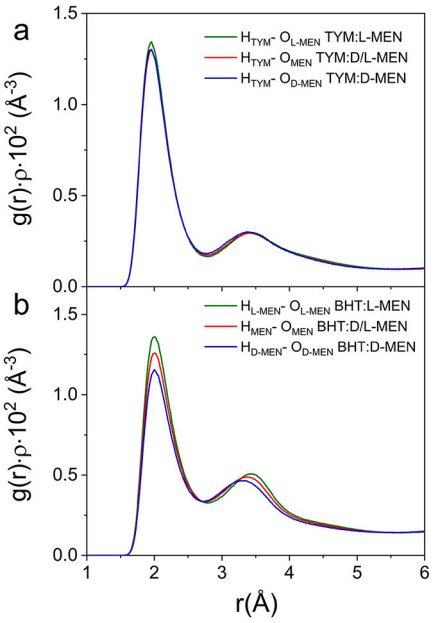

Fig. 4. Radial distribution functions multiplied by the numerical density of the observed atoms, $g(r)\rho$'s, calculated from the MD simulations at 298 K for the intermolecular a) H_{TYM}-O_{MEN} distribution in the TYM:MEN 1:1 mixtures and b) H_{MEN}-O_{MEN} distribution in the BHT:MEN 1:3 mixtures with MEN = L-MEN (green), D/L-MEN (red), and D-MEN (blue).

same trend observed for the pure enantiomers is found. Conversely, in the TYM:MEN 1:1 system, the functions are nearly superimposable for the TYM-TYM (Fig. S5e) and TYM-MEN (Fig. S5f) interactions, while the MEN-MEN one (Fig. S5d) maintains the behavior observed in the pure systems.

3.4. The long-range structural picture

The previous structural analyses have shown that the TYM:MEN system is unaffected by the choice of the MEN enantiomer, in contrast with the BHT:MEN mixtures, which display some variations in the microscopic molecular organization. The focus now shifts to investigating whether this behavior persists in the structural arrangement on a larger scale length. To this purpose, SWAXS data were collected on the TYM:MEN 1:1 and BHT:MEN 1:3 mixtures at variance with the MEN precursor and compared in Figs. 5a and c, respectively. At first glance, the scattering profiles look similar between the two kinds of eutectics, especially for what concerns the main peak in the WAXS region ($q \geq 0.5$ Å^{-1}). A diagnostic feature is the pre-peak occurring at about 0.6 Å^{-1} in both systems, which corresponds to a ~10 Å distance in the real space.

Such a contribution was previously associated with the electron-density inhomogeneities promoted by the H-bonding aggregation typical of terpenoid-based eutectics. [74,35,75,76] This results in recurring distances between pools of higher electron density, represented by the oxygen atoms, intercalated by regions of lower density, consisting of the carbon bodies of the constituents. This picture can be appreciated from a qualitative point of view by the MD snapshots of the simulation boxes reported in Fig. 5, where the oxygen atoms are illustrated as red surfaces, while the carbon and hydrogen atoms are in gray. It is evident that there are no discernible differences between these patterns upon changing the enantiomer in both the TYM- (Fig. 5b) and BHT-based (Fig. 5d) mixtures, as the higher electron density regions exhibit a similar distribution across all considered systems. In addition, the spectra are almost superimposable through all the explored q-range (Fig. 5a and c). This applies also to the low angular values in the SAXS region ($q \leq 0.5$ Å^{-1}), which is sensitive towards electron density inhomogeneities on a larger scale length. A flat profile is obtained in all cases, which means the formation of no longer-range structuring into distinctive domains, in agreement with many other DESs. [77,27,76] The whole result highlights that the selection of a specific MEN enantiomer has no observable impact on the intermediate- and long-range arrangement in both the TYM:MEN 1:1 DES and BHT:MEN 1:3 ideal eutectic. In order to have a proof of the validity of the MD results, theoretical SWAXS spectra of the BHT:MEN 1:3 and TYM:MEN 1:1 systems have been calculated from the simulation trajectories using the TRAVIS software. The results are shown in Fig. S7 for all the systems. The overall agreement between the experimental and theoretical curves is good even if the intensity of the pre-peak occurring at 0.6 Å^{-1} is not properly reproduced by the calculations. However, the presence of a bump is clearly detected in the BHT:MEN 1:3 systems and the intensity of this peak increases in the TYM:MEN 1:1 mixtures, in agreement with the experimental determination.

4. Conclusions

TYM:MEN 1:1 and BHT:MEN 1:3 eutectic mixtures were investigated to understand the influence of the precursor chirality on their thermal and structural properties. The characterization of MEN single enantiomeric and racemic compounds was first carried out and showed that D/L-MEN melts at a significantly lower temperature than L-MEN and D-MEN, as determined by DSC measurements. Raman spectroscopy and MD simulations showed that self-interaction among MEN molecules is more favorable in the melt phase of L-MEN than in D/L- and D-MEN. This trend is preserved in mixtures with BHT, as the MP of the BHT:D/L-MEN mixture is lower than that of the BHT/L-MEN and BHT/D-MEN eutectics. A higher extent of H-bonding among the MEN molecules is observed for the BHT:L-MEN system. This behavior is explained by the poor interactions that take place between the MEN molecules and the sterically hindered BHT, where the single enantiomers maintain their own interactions with the chiral molecules in the eutectic mixture.

A different situation has been found for the TYM:MEN mixtures, where the COSMO-RS solvation model predicts an almost identical SLE independently of the MEN precursor. Raman and MD results showed that the main structure-driving interaction, *i.e.*, the TYM-MEN donor-receptor H-bond, is similar in the three systems, and the non-chiral TYM molecule has been found not to be sensitive towards the MEN chirality. Moreover, SWAXS data evidenced that the selection of a specific enantiomer has no observable impact on the intermediate- and long-range structural arrangement in both TYM:MEN 1:1 and BHT:MEN 1:3.

In terms of the use of a chiral solvent, some guidelines can be traced according to the obtained knowledge. The high affinity between the components in a DES could compete against the interactions with other substrate molecules and hinder the application as a chiral solvent. The other side of the coin is that the indiscriminate employment of a chiral precursor provokes no substantial alteration of the overall thermal and structural properties. On the other hand, the weaker interactions between the parent molecules help preserve the behavior of the optically active component in an ideal eutectic solvent, which appears more suitable for enantioselective purposes.

CRediT authorship contribution statement

Giorgia Mannucci: Writing – review & editing, Writing – original draft, Formal analysis, Data curation, Conceptualization. **Matteo Busato:** Writing – review & editing, Writing – original draft, Supervision, Formal analysis, Data curation, Conceptualization. **Eva Pietropaoli:** Investigation, Data curation. **Matteo Palluzzi:** Investigation, Formal analysis, Data curation. **Paolo Casu:** Investigation, Formal analysis, Data curation. **Angela Capocefalo:** Investigation, Formal analysis, Data curation. **Claudia Fasolato:** Writing – review & editing, Investigation, Formal analysis, Data curation, Conceptualization. **Paolo Postorino:** Writing – review & editing, Supervision, Methodology, Conceptualization. **Paola D'Angelo:** Writing – review & editing, Writing –

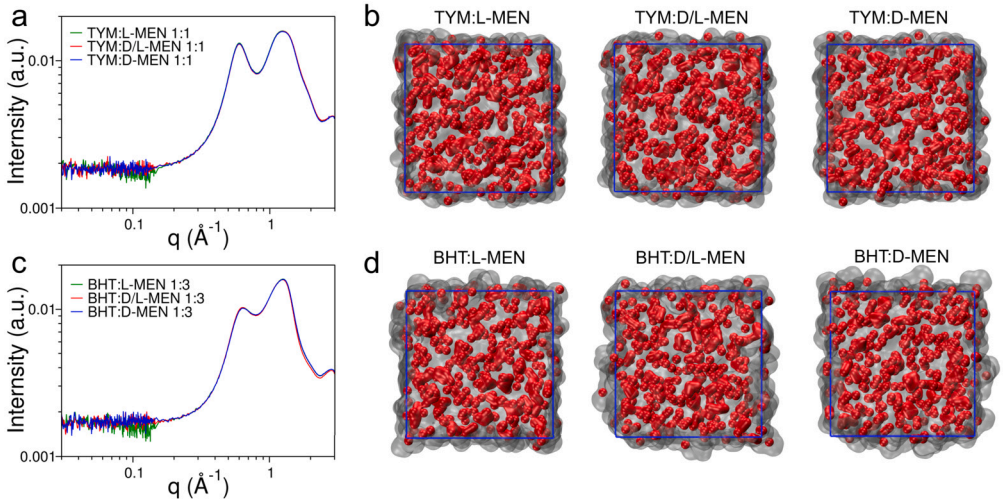

Fig. 5. Experimental SWAXS spectra in double-logarithmic scale collected at 298 K for the a) TYM:MEN 1:1 and c) BHT:MEN 1:3 mixtures with MEN = L-MEN (green), D/L-MEN (red), and D-MEN (blue). Snapshots of the simulation boxes taken from the final configuration of the MD simulations performed at 298 K for the b) TYM:MEN 1:1 and d) BHT:MEN 1:3 mixtures. Oxygen atoms are visualized as red surfaces, while carbon and hydrogen atoms are shown in transparent gray. Box edges are highlighted by blue lines.

original draft, Supervision, Funding acquisition, Data curation, Conceptualization.

Declaration of competing interest

The authors declare that they have no known competing financial interests or personal relationships that could have appeared to influence the work reported in this paper.

Acknowledgements

Part of the calculations was performed on the Leonardo system of the CINECA supercomputing center (grant IsCa8_PAREDES). The CoSAXS beamline of MAX IV Laboratory and its staff are acknowledged for synchrotron radiation beam time. The authors acknowledge the European Union-NextGenerationEU under the Italian Ministry of University and Research (MUR), Network 4 Energy Sustainable Transition - NEST project - CUP B53C22004070006, the project ECS 0000024 Rome Technopole, - CUP B83C22002820006 and the Italian Ministry of University and Research (MUR) for the PRIN project “MOF-MTM: tailoring Metal-Organic Frameworks for the direct Methane To Methanol conversion under mild conditions” number 2022SFC459.

Appendix A. Supplementary material

Supplementary material related to this article can be found online at https://doi.org/10.1016/j.molliq.2025.127676.

Data availability

Data will be made available on request.

References

[1] E.L. Smith, A.P. Abbott, K.S. Ryder, Chem. Rev. 114 (2014) 11060–11082.
[2] B.B. Hansen, S. Spittle, B. Chen, D. Poe, Y. Zhang, J.M. Klein, A. Horton, L. Adhikari, T. Zelovich, B.W. Doherty, B. Gurkan, E.J. Maginn, A. Ragauskas, M. Dadmun, T.A. Zawodzinski, G.A. Baker, M.E. Tuckerman, R.F. Savinell, J.R. Sangoro, Chem. Rev. 121 (2021) 1232–1285.
[3] M.A. Martins, S.P. Pinho, J.A. Coutinho, J. Solution Chem. 48 (2019) 962–982.
[4] A.J. Peloquin, J.M. McCollum, C.D. McMillen, W.T. Pennington, Angew. Chem. Int. Ed. 60 (2021) 22983–22989.
[5] M. Busato, G. Mannucci, V. Di Lisio, A. Martinelli, A. Del Giudice, A. Tofoni, C. Dal Bosco, V. Migliorati, A. Gentili, P. D’Angelo, ACS Sustain. Chem. Eng. 10 (2022) 6337–6345.
[6] M. Busato, G. Mannucci, L.A. Rocchi, M.E. Di Pietro, A. Capocefalo, E. Zorzi, P. Casu, D. Veclani, F. Castiglione, A. Mele, et al., ACS Sustain. Chem. Eng. 11 (2023) 8988–8999.
[7] A. van den Bruinhorst, C. Corsini, G. Depraetère, N. Cam, A.A. Padua, M. Costa Gomes, Faraday Discuss. (2024).
[8] D.J. Van Osch, C.H. Dietz, S.E. Warrag, M.C. Kroon, ACS Sustain. Chem. Eng. 8 (2020) 10591–10612.
[9] C. Dal Bosco, F. Mariani, A. Gentili, Molecules 27 (2022) 908.
[10] B.D. Ribeiro, C. Florindo, L.C. Iff, M.A. Coelho, I.M. Marrucho, ACS Sustain. Chem. Eng. 3 (2015) 2469–2477.
[11] C. Dal Bosco, V. Di Lisio, P. D’Angelo, A. Gentili, ACS Sustain. Chem. Eng. 9 (2021) 8170–8178.
[12] Z. Yuan, H. Liu, W.F. Yong, Q. She, J. Esteban, Green Chem. 24 (2022) 1895–1929.
[13] N. Schaeffer, J.H.F. Conceição, M.A.R. Martins, M.C. Neves, G. Pérez-Sánchez, J.R.B. Gomes, N. Papaiconomou, J.A.P. Coutinho, Green Chem. 22 (2020) 2810–2820.
[14] G. Zante, M. Boltoeva, Sustain. Chem. 1 (2020) 238–255.
[15] N. Schaeffer, M.A.R. Martins, C.M.S.S. Neves, S.P. Pinho, J.A.P. Coutinho, Chem. Commun. 54 (2018) 8104–8107.
[16] D.J.G.P. Van Osch, D. Parmentier, C.H.J.T. Dietz, A. van den Bruinhorst, R. Tuinier, M.C. Kroon, Chem. Commun. 52 (2016) 11987–11990.
[17] E. Tereshatov, M.Y. Boltoeva, C. Folden, Green Chem. 18 (2016) 4616–4622.
[18] M.A. Martins, L.P. Silva, N. Schaeffer, D.O. Abranches, G.J. Maximo, S.P. Pinho, J.A. Coutinho, ACS Sustain. Chem. Eng. 7 (2019) 17414–17423.
[19] S. Zwenger, C. Basu, Biotechnol. Mol. Biol. Rev. 3 (2008) 1.
[20] P.A. Shah, V. Chavda, D. Hirpara, V.S. Sharma, P.S. Shrivastav, S. Kumar, J. Mol. Liq. 390 (2023) 123171.
[21] E. Silva, F. Oliveira, J.M. Silva, R.L. Reis, A.R.C. Duarte, Curr. Res. Chem. Biol. 1 (2021) 100003.
[22] V. Vanoli, J. Pietrowska, G. de Araujo Lima e Souza, M.E. Di Pietro, F. Briatico Vangosa, A. Mele, F. Castiglione, ACS Appl. Eng. Mater. 2 (2024) 388–396.
[23] M. Gohel, S. Nagori, Indian J. Pharm. Sci. 71 (2009) 622.
[24] Q. Shen, X. Li, W. Li, X. Zhao, AAPS PharmSciTech 12 (2011) 1044–1049.
[25] Y. Corvis, P. Négrier, S. Massip, J.-M. Leger, P. Espeau, CrystEngComm 14 (2012) 7055–7064.
[26] T.A. Hopkins, L. VandenElzen, B.P. Nelson, V. Vaid, J. Brickley, P. Ariza, G. Whitacre, I. Patel, O. Gooch, M. Bechman, C. Jordan, Ind. Eng. Chem. Res. 62 (2023) 1606–1613.
[27] E.K. Bathke, D.T. Bowron, I. Manasi, K.J. Edler, J. Mol. Liq. 402 (2024) 124735.
[28] P. Jahanbakhsh-Bonab, G. Pazuki, J.J. Sardroodi, S.M. Dehnavi, Phys. Chem. Chem. Phys. 25 (2023) 17547–17557.
[29] S. Arnaboldi, A. Mezzetta, S. Grecchi, M. Longhi, E. Emanuele, S. Rizzo, F. Arduini, L. Micheli, L. Guazzelli, P.R. Mussini, Electrochim. Acta 380 (2021) 138189.
[30] S. Grecchi, S. Arnaboldi, S. Rizzo, P.R. Mussini, Curr. Opin. Electrochem. 30 (2021) 100810.
[31] T. Palomba, G. Ciancaleoni, T. Del Giacco, R. Germani, F. Ianni, M. Tiecco, J. Mol. Liq. 262 (2018) 285–294.
[32] M. Tiecco, D.A. Alonso, D.R. Ñíguez, G. Ciancaleoni, G. Guillena, D.J. Ramòn, A.A. Bonillo, R. Germani, J. Mol. Liq. 313 (2020) 113573.
[33] B. Nelson, L. VandenElzen, G. Whitacre, T.A. Hopkins, ChemPhotoChem 5 (2021) 1071–1078.
[34] C.R. Wright, L. VandenElzen, T.A. Hopkins, J. Phys. Chem. B 122 (2018) 8730–8737.

[35] N. Schaeffer, D.O. Abranches, L.P. Silva, M.A. Martins, P.J. Carvalho, O. Russina, A. Triolo, L. Paccou, Y. Guinet, A. Hedoux, et al., ACS Sustain. Chem. Eng. 9 (2021) 2203–2211.
[36] F. Ripanti, C. Fasolato, F. Mazzarda, S. Palleschi, M. Ceccarini, C. Li, M. Bignami, E. Bodo, S.E. Bell, F. Mazzei, P. Postorino, Anal. Chem. 93 (2021) 10825–10833.
[37] T.S. Plivelic, A.E. Terry, R. Appio, K. Theodor, K. Klementiev, AIP Conf. Proc. 2054 (2019) 030013.
[38] M. Sztucki, T. Narayanan, J. Appl. Crystallogr. 40 (2007) s459–s462.
[39] K. Manalastas-Cantos, P.V. Konarev, N.R. Hajizadeh, A.G. Kikhney, M.V. Petoukhov, D.S. Molodenskiy, A. Panjkovich, H.D.T. Mertens, A. Gruzinov, C. Borges, C.M. Jeffries, D.I. Svergun, D. Franke, J. Appl. Crystallogr. 54 (2021) 343–355.
[40] L. Martínez, R. Andrade, E. Birgin, J. Martínez, J. Comput. Chem. 30 (2009) 2157–2164.
[41] G. Popov, K. Kolarov, C. Veltschev, K. Manolov, Monatsh. Chem. 108 (1977) 159–161.
[42] B. Hess, H. Bekker, H.J. Berendsen, J.G. Fraaije, J. Comput. Chem. 18 (1997) 1463–1472.
[43] M.J. Abraham, T. Murtola, R. Schulz, S. Páll, J.C. Smith, B. Hess, E. Lindahl, SoftwareX 1 (2015) 19–25.
[44] W. Humphrey, A. Dalke, K. Schulten, J. Mol. Graph. 14 (1996) 33–38.
[45] W.L. Jorgensen, D.S. Maxwell, J. Tirado-Rives, J. Am. Chem. Soc. 118 (1996) 11225–11236.
[46] M. Jasik, B. Szefczyk, J. Mol. Model. 22 (2016) 1–9.
[47] T. Darden, D. York, L. Pedersen, J. Chem. Phys. 98 (1993) 10089–10092.
[48] U. Essmann, L. Perera, M.L. Berkowitz, T. Darden, H. Lee, L.G. Pedersen, J. Chem. Phys. 103 (1995) 8577–8593.
[49] C.M. Breneman, K.B. Wiberg, J. Comput. Chem. 11 (1990) 361–373.
[50] A.D. Becke, J. Chem. Phys. 96 (1992) 2155–2160.
[51] M.e. Frisch, G. Trucks, H.B. Schlegel, G. Scuseria, M. Robb, J. Cheeseman, G. Scalmani, V. Barone, G. Petersson, H. Nakatsuji, et al., Gaussian 16 (2016).
[52] TURBOMOLE V4.5.2 2019, a development of University of Karlsruhe and Forschungszentrum Karlsruhe GmbH, 1989-2007, TURBOMOLE GmbH, since 2007, available from http://www.turbomole.com, 2007.
[53] J.P. Perdew, Phys. Rev. B 33 (1986) 8822.
[54] A.D. Becke, Phys. Rev. A 38 (1988) 3098.
[55] F. Weigend, M. Häser, H. Patzelt, R. Ahlrichs, Chem. Phys. Lett. 294 (1998) 143–152.
[56] F. Weigend, R. Ahlrichs, PCCP 7 (2005) 3297–3305.
[57] http://www.3ds.com.
[58] Z.J. Li, M.T. Zell, E.J. Munson, D.J. Grant, J. Pharm. Sci. 88 (1999) 337–346.
[59] D. Lin-Vien, N.B. Colthup, W.G. Fateley, J.G. Grasselli, The Handbook of Infrared and Raman Characteristic Frequencies of Organic Molecules, Elsevier, 1991.
[60] B.T. Lutz, M.H. Langoor, J.H. van der Maas, Vib. Spectrosc. 18 (1998) 111–121.
[61] F. Palombo, M. Paolantoni, P. Sassi, A. Morresi, R.S. Cataliotti, J. Mol. Liq. 125 (2006) 139–146.
[62] M. Paolantoni, P. Sassi, A. Morresi, R.S. Cataliotti, J. Raman Spectrosc. 37 (2006) 528–537.
[63] G. Teixeira, D.O. Abranches, O. Ferreira, J.A. Coutinho, Ind. Eng. Chem. Res. 62 (2023) 14638–14647.
[64] R. Böhmer, C. Gainaru, R. Richert, Phys. Rep. 545 (2014) 125–195.
[65] J. Kiefer, S. Wagenfeld, D. Kerlé, Spectrochim. Acta, Part A, Mol. Biomol. Spectrosc. 189 (2018) 57–65.
[66] P. Kalhor, Q.-Z. Li, Y.-Z. Zheng, Z.-W. Yu, J. Phys. Chem. A 124 (2020) 6177–6185.
[67] A. Triolo, F. Lo Celso, O. Russina, J. Mol. Liq. 372 (2023) 121151.
[68] A. Serva, V. Migliorati, A. Lapi, G. Aquilanti, A. Arcovito, P. D'Angelo, Phys. Chem. Chem. Phys. 18 (2016) 16544–16554.
[69] D. Herschlag, M.M. Pinney, Biochem. 57 (2018) 3338–3352.
[70] A. Alhadid, C. Jandl, L. Mokrushina, M. Minceva, Cryst. Growth Des. 21 (2021) 6083–6091.
[71] C. D'Hondt, D. Morineau, J. Mol. Liq. 365 (2022) 120145.
[72] G. Mannucci, G. Teixeira, F.H.B. Sosa, M. Palluzzi, M. Busato, J.A. Coutinho, P. D'Angelo, ACS Sustain. Chem. Eng. 12 (7) (2024) 2862–2870.
[73] D.O. Abranches, M.A. Martins, L.P. Silva, N. Schaeffer, S.P. Pinho, J.A. Coutinho, Chem. Commun. 55 (2019) 10253–10256.
[74] A. Malik, H.K. Kashyap, Phys. Chem. Chem. Phys. 23 (2021) 3915–3924.
[75] G. Mannucci, M. Busato, A. Tofoni, P. D'Angelo, J. Mol. Liq. 375 (2023) 121302.
[76] G. Mannucci, A. Tofoni, M. Busato, P. D'Angelo, J. Mol. Liq. 394 (2024) 123746.
[77] M. Busato, V. Di Lisio, A. Del Giudice, P. Tomai, V. Migliorati, L. Galantini, A. Gentili, A. Martinelli, P. D'Angelo, J. Mol. Liq. 331 (2021) 115747.